Ancestral absence of electron transport chains in Patescibacteria and DPANN

Jacob P. Beam[1], Eric D. Becraft[1,15], Julia M. Brown[1], Frederik Schulz[2], Jessica K. Jarett[2,16], Oliver Bezuidt[1], Nicole J. Poulton[1], Kayla Clark[1,17], Peter F. Dunfield[3], Nikolai V. Ravin[4], John R. Spear[5], Brian P. Hedlund[6], Konstantinos A. Kormas[7], Stefan M. Sievert[8], Mostafa S. Elshahed[9], Hazel A. Barton[10], Matthew B. Stott[11], Jonathan A. Eisen[12], Duane P. Moser[13], Tullis C. Onstott[14], Tanja Woyke[2], and Ramunas Stepanauskas[1*]

[1]Bigelow Laboratory for Ocean Sciences, East Boothbay, Maine, USA, 04544

[2]Department of Energy Joint Genome Institute, Walnut Creek, California, USA, 94598

[3]University of Calgary, Calgary, AB, Canada, T2N 1N4

[4]Institute of Bioengineering, Research Center of Biotechnology of the Russian Academy of Sciences, Moscow, 119071, Russia

[5]Civil and Environmental Engineering, Colorado School of Mines, Golden, Colorado 80401

[6]School of Life Sciences, University of Nevada Las Vegas, Las Vegas, NV, 89154, USA. Nevada Institute of Personalized Medicine, University of Nevada Las Vegas, Las Vegas, NV, USA, 89154

[7]Department of Ichthyology and Aquatic Environment, University of Thessaly, 38446, Volos, Greece

[8]Biology Department, Woods Hole Oceanographic Institution, Woods Hole, MA, USA, 02543

[9]Department of Microbiology and Molecular Genetics, Oklahoma State University, Stillwater, Oklahoma, USA

[10]Department of Biology, University of Akron, Akron, OH 44325

[11]School of Biological Sciences, University of Canterbury, Christchurch, 8041 New Zealand.

[12]University of California Davis, Davis, CA, USA, 95616

[13]Desert Research Institute, Las Vegas, Nevada, USA, 89119

[14]Princeton University, Princeton, New Jersey, USA, 08544

Current address:

[15]University of North Alabama, Florence, AL, USA, 35632

[16]AnimalBiome, Oakland, CA, USA, 94609

[17]U.S. Army Engineer Research and Development Center, US Army Corp of Engineers, Vicksburg, Mississippi, 39180

*To whom correspondence should be addressed: rstepanauskas@bigelow.org

Abstract

Recent discoveries suggest that the candidate superphyla Patescibacteria and DPANN constitute a large fraction of the phylogenetic diversity of Bacteria and Archaea. Their small genomes and limited coding potential have been hypothesized to be ancestral adaptations to obligate symbiotic lifestyles. To test this hypothesis, we performed cell-cell association, genomic, and phylogenetic analyses on 4,829 individual cells of Bacteria and Archaea from 46 globally distributed surface and subsurface field samples. This confirmed the ubiquity and abundance of Patescibacteria and DPANN in subsurface environments, the small size of their genomes and cells, and the divergence of their gene content from other Bacteria and Archaea. Our analyses suggest that most Patescibacteria and DPANN in the studied subsurface environments do not form specific physical associations with other microorganisms. These data also suggest that their unusual genomic features and prevalent auxotrophies may be a result of minimal cellular energy transduction mechanisms that potentially precede the evolution of respiration, thus relying solely on fermentation for energy conservation.

Keywords: Bacteria, Archaea, evolution, single amplified genome, energy, auxotrophy, symbiosis, electron transport chain, fermentation, respiration, oxidoreductases

Introduction

Cultivation-independent research tools have revealed the coding potential of numerous, deep branches of Bacteria and Archaea that were unknown until recently (Wrighton et al., 2012; Rinke et al., 2013; Brown et al., 2015; Castelle et al., 2015) Among them, the candidate bacterial superphylum Patescibacteria (also known as Candidate Phyla Radiation, CPR) and archaeal superphylum DPANN have garnered particular attention, as they appear to constitute a large fraction of microbial diversity in subsurface and various other environments (Brown et al., 2015; Hug et al., 2016; Dombrowski et al., 2019). Patescibacteria and DPANN are characterized by small genomes and cell sizes, and predicted minimal biosynthetic and metabolic potential (Wrighton et al., 2012; Luef et al., 2015; Castelle and Banfield, 2018). They also appear to have slow metabolism, as indicated by low per-cell ribosome counts (Luef et al., 2015) and slow estimated genome replication rates (Brown et al., 2016). Host-dependent endo- and ecto-symbioses have been observed in several Patescibacteria (Gong et al., 2014; He et al., 2015; Cross et al., 2019) and the Nanoarchaeota and Nanohaloarchaeota phyla within DPANN (Huber et al., 2002; Podar et al., 2013; Munson-McGee et al., 2015; Jarett et al., 2018; Hamm et al., 2019). As a result, it has been posited that the unusual biological features of Patescibacteria and DPANN reflect ancestral adaptations to symbiotic lifestyles (Castelle et al., 2018; Dombrowski et al., 2019). However, direct evidence of symbiosis in Patescibacteria and DPANN is limited to a small number of narrow phylogenetic groups inhabiting surface environments and, in the case of Patescibacteria, dependent on eukaryotic hosts (Gong et al., 2014) or eukaryotic host systems (He et al., 2015; Cross et al., 2019) (i.e., mammalian oral cavities), which suggests relatively recent adaptations.

Here, we performed physical cell-cell association, genomic, and phylogenetic analyses on 4,829 of individual microbial cells from 46 globally distributed and environmentally diverse locations to gain additional insights into the unusual biological features of Patescibacteria and DPANN. Consistent with prior reports, we found these two superphyla abundant in many subsurface environments, and also confirm their consistently small cell and genome sizes. Our single cell genomic and biophysical observations do not support the prevailing view that Patescibacteria and DPANN are dominated by symbionts (Castelle et al., 2018; Dombrowski et al., 2019). Instead, based on the apparent lack of genes for complete electron transport systems, we hypothesize that these two superphyla have not evolved the capacity for respiration and therefore rely on fermentative metabolisms for energy conservation. Although complex metabolic interdependencies are a rule rather than exception in natural microbiomes (Zengler and Zaramela, 2018), the predicted fermentative energy conservation and limited biosynthetic potential (Castelle et al., 2018; Dombrowski et al., 2019) of Patescibacteria and DPANN may define a highly communal lifestyle of these two superphyla and provide explanation for the extreme difficulty in obtaining them in pure culture.

Materials and Methods

Field sample collection

Field samples were collected from a global set of diverse environments that were found to contain candidate phyla of Bacteria and Archaea in prior studies (Rinke et al., 2013; Thomas et al., 2013; Moser et al., 2015; Becraft et al., 2017; Hershey et al., 2018; Sackett, 2018; Sackett et al., 2018, 2019). Immediately after collection, samples were amended with sterile 5% glycerol

and 1 mM EDTA (final concentrations) and stored at -80 °C. Field sample metadata is located with each individual SAG in Table S1.

Single amplified genome (SAG) generation, sequencing, and *de novo* assembly

SAG generation and sequencing were performed by Bigelow Laboratory for Ocean Sciences Single Cell Genomics Center (SCGC) and U.S. Department of Energy Joint Genome Institute (JGI) (Table S1). At SCGC, field samples were stained with SYTO-9 nucleic acids stain (Thermo Fisher Scientific), separated using fluorescence-activated cell sorting (FACS), lysed using a combination of freeze-thaw and alkaline treatment, and their genomic DNA was amplified using WGA-X in a cleanroom, as previously described (Stepanauskas et al., 2017). For sorting of cells with active oxidoreductases, the Beatrix field sample (plate AG-274) was pre-incubated with the RedoxSensor Green stain (Thermo Fisher Scientific) following manufacturer's instructions. During cell sorting, cell size estimates were performed using calibrated index FACS (Stepanauskas et al., 2017). All SAGs generated at SCGC were subject to Low Coverage Sequencing (LoCoS) using a modified Nextera library preparation protocol and NextSeq 500 (Illumina) sequencing instrumentation (Stepanauskas et al., 2017). This resulted in a variable number of 2x150bp reads per SAG, with an average of ~300k. The reads were de novo assembled using a customized workflow utilizing SPAdes (Bankevich et al., 2012), as previously described (Stepanauskas et al., 2017). The quality of the sequencing reads was assessed using FastQC and the quality of the assembled genomes (contamination and completeness) was assessed using checkM (Parks et al., 2015) and tetramer frequency analysis (Woyke et al., 2009). This SAG generation, sequencing and assembly workflow was previously evaluated for assembly errors using three bacterial benchmark cultures with diverse genome complexity and

GC content (%), indicating no non-target and undefined bases in the assemblies and average frequencies of mis-assemblies, indels and mismatches per 100 kbp being 1.5, 3.0 and 5.0 (Stepanauskas et al., 2017). Functional annotation was first performed using Prokka (Seemann, 2014) with default Swiss-Prot databases supplied by the software. Prokka was run a second time with a custom protein annotation database built from compiling Swiss-Prot (Bateman et al., 2017) entries for Archaea and Bacteria. The uniquely barcoded sequencing libraries of SAGs belonging to candidate divisions were combined, in equal proportions, into 48-library pools and shipped to JGI for deeper sequencing with NextSeq 500 (Illumina) in 2x150 bp mode. Quality filtering of raw reads was performed with BBTools v.37, read normalization with BBNorm, and error correction with Tadpole (http://bbtools.jgi.doe.gov). The resulting reads were assembled with SPAdes (Nurk et al., 2013) (v3.9.0, --phred-offset 33 –sc -k 22,55,95 –12), and 200 bp was trimmed from the ends of assembled contigs, after which contigs with read coverage < 2 or < 2 kbp in length were discarded. Assemblies were annotated according to IMG standard protocols (Huntemann et al., 2016; Chen et al., 2019). All SAGs are publicly available in IMG/M (Chen et al., 2019), and can be found under their GOLD analysis project identifiers in Table S1.

Identification of heterogenous DNA sources

The 16S ribosomal RNA gene was identified in SAGs by searching them individually using cmsearch, which is part of the infernal package (Nawrocki and Eddy, 2013), using the bacterial 16S rRNA Rfam covariance model (rfam.xfam.org/family/RF00177). This method is particularly helpful in predicting 16S rRNA genes in Patescibacteria and DPANN, which can often have introns in their 16S rRNA genes (Brown, 2015). Taxonomic assignments to these 16S rRNA genes were conducted using “classify.seqs” within mothur (Schloss et al., 2009) version

1.41.3 against the Silva 132 reference database and taxonomy file (Quast et al., 2013). The resulting taxonomy file was used to search for SAGs that contained two 16S rRNA genes that had different taxonomic phylum-level assignments and were marked as putative co-sorts; those that did not have two 16S rRNA genes were marked as single sorts. The checkM (Parks et al., 2015) contamination estimates were used to determine SAGs that had high values of potential genome admixture (e.g., two different cellular origins). A Chi-squared test was performed in R using the "chisq.test" function on potential co-sorted and single sorted SAGs, and Pearson's residuals were retrieved from the output of this test and used to calculate the percent contribution to each X^2 statistic, and plotted using the "corrplot" package in R Studio.

Genomes from prior studies

A total of 1,025 publicly available SAGs, metagenome bins, and isolate genomes (Table S2) were used in this study from the Integrated Microbial Genomes and Microbiomes (IMG/M) database (Chen et al., 2019) (genomes accessed April 2018). These genomes were selected by clustering the RNA polymerase COG0086 protein sequence at 70% identity, and if there were similar genomes at the 70% identity threshold, the one with the most complete set of 56 single copy proteins was chosen as representative. Phylum-level classification and symbiotic lifestyle assignments were exported from IMG/M. In cases were IMG/M lacked lifestyle assignments, manual literature searches of organism names were used to determine whether they have documented symbiotic relationships.

184 Concatenated single copy protein phylogeny

185 A set of 56 universal single copy marker proteins (Eloe-Fadrosh et al., 2016; Yu et al.,
186 2017) was used to build a phylogenetic tree for the newly generated SAGs and MAGs and a
187 representative set of bacteria and archaea based on publicly available microbial genomes in
188 IMG/M (Chen et al., 2019) (genomes accessed in April 2018). Marker proteins were identified
189 with hmmsearch (Eddy, 2011) version 3.1b2, using a specific Hidden Markov Model for each of
190 the markers. Genomes for which 5 or more different marker proteins could be identified were
191 included in the tree. For every marker protein, alignments were built with MAFFT (Nakamura et
192 al., 2018) v7.294b and subsequently trimmed with BMGE (Criscuolo and Gribaldo, 2010) v1.12
193 using BLOSUM30. Single protein alignments were concatenated and maximum likelihood
194 phylogenies inferred with FastTree2 (Price et al., 2010) using the options: -spr 4 -mlacc 2 -
195 slownni -lg (for archaea) and -spr 4 -mlacc 2 -slownni -lg (for bacteria).
196
197 Clusters of orthologous groups principal components analysis
198 Clusters of orthologous groups (COGs) were assigned to SAG (Table S1) and reference
199 genome (Table S2) predicted protein sequences using reverse position-specific blast (rpsblast)
200 (Altschul et al., 1997) with an e-value cutoff of 1e-5 and the cdd2cog script
201 (https://github.com/aleimba/bac-genomics-scripts/tree/master/cdd2cog). Genomes that were used
202 for the principal component analysis (PCA) had completeness estimates greater than or equal to
203 30%, and contained 16S rRNA genes for unambiguous phylum-level classification. Eigenvector
204 values were calculated in RStudio (RStudio Team, 2016) version 1.1.463 using the cmdscale
205 function from relative abundances of the different COG categories expressed as a percent out of
206 the total number of assigned COGs. PCA plots were visualized with ggplot2 (Wickham, 2016) in

RStudio (RStudio Team, 2016). A Wilcoxon test was performed in RStudio using the "wilcox.test" function to determine statistical differences between principal components among the different clusters discussed in the main text. The color scheme for these plots is based on the Color Universal Design (https://jfly.uni-koeln.de/color/), and should be distinguishable by all types of vision. This color scheme was used throughout all the figures in the manuscript.

Coding sequence density

Coding sequences (CDS) for SAGs and reference genomes were predicted using Prodigal (Hyatt et al., 2010) version 2.6.3. The initial analysis of prokka CDS density revealed that numerous SAGs and reference genomes had very low coding densities. Prokka utilizes the code 11 translation table by default, and many of these genomes could potentially use stop codons in place of canonical codons (Wrighton et al., 2012; Rinke et al., 2013). We determined the correct translation table to utilize for each genome by comparing the total CDS length from Code 11 and Code 25 predictions, and if the Code 11 total CDS length was greater than the Code 25 total CDS length, then the total length from Code 11 was used in the coding density calculation. If the opposite was true, then the Code 25 total CDS length was used. The coding density was calculated by dividing the total CDS sequence by the total assembly size.

Oxygen reductase identification

A published heme copper oxidase subunit I database (Sousa et al., 2011) from bacteria and archaea was used as a database with blastp (Altschul et al., 1990) with an e-value cutoff of 1e-10 using the SAG and reference genomes as queries. The original database file had to be de-replicated (i.e., removing 100% identical sequences) using the dedupe.sh script, which is part of

the BBMap package (https://github.com/BioInfoTools/BBMap). The sole crystal structure sequence for the bd-ubiquinol oxidase subunit A from *Geobacillus thermodentrificans* (Safarian et al., 2016) was used as a database for a blastp (Altschul et al., 1990) search using the SAGs and reference genomes as queries with an e-value cutoff of 1e-10.

Oxygen reductase horizontal gene transfer

The protein sequences identified from the above section were retrieved from SAGs using the grep function from the list of sequence file headers from the above analysis in the SeqKit package (Shen et al., 2016). Reference protein sequences for Patescibacteria were retrieved via the blastp server using the Patescibacteria SAG HCO sequences as queries and selecting for hits only from sequences that were assigned to Patescibacteria and/or Candidate Phyla Radiation. Other reference sequences for Patescibacteria were retrieved by manual literature searches from relevant studies (Nelson and Stegen, 2015; León-Zayas et al., 2017; Castelle et al., 2018). The search for Patescibacteria HCOs revealed that they only encoded for the low-affinity Type A HCO, and all subsequent phylogenetic analyses focused solely on this HCO type. The multi-fasta file containing all HCO sequences was filtered for sequences that were greater than 400 amino acids in length, and aligned with mafft (Nakamura et al., 2018) using the "--auto" option and the resulting alignment was trimmed with trimal (Capella-Gutiérrez et al., 2009) to remove gaps using the "-gappyout" option. A maximum likelihood phylogenetic tree was created using FastTree (Price et al., 2010) using the LG model of amino acid evolution. No DPANN genome to date has had a positive identification of an HCO subunit I. The methodology for the HCO phylogeny was repeated for the bd-ubiquinol oxygen reductases. Phylogenetic trees were visualized and annotated using the online Interactive Tree of Life tool (Letunic and Bork, 2019).

253

254 Oxidoreductase annotation and abundance

255 Enzyme Commission 1 (EC1) class family proteins (i.e., oxidoreductases) were predicted from
256 the SAGs and reference genomes using the prokka "genome.tsv" annotation files. The total
257 number of predicted protein sequences annotated as EC1 for each genome was divided by the
258 total number of predicted protein sequences to provide the percent of protein encoding genes that
259 were predicted to be oxidoreductases. This allows for a direct comparison of all the genomes that
260 exhibited wide ranges in completeness estimates.

261

262 KEGG orthology assignment of electron transport chain proteins

263 The Kyoto Encyclopedia of Gene and Genomes (KEGG) orthology (KO) annotations were
264 assigned using KofamKOALA (Aramaki et al., 2019), which uses hmmsearch (Eddy, 2011)
265 against curated hidden Markov model (HMM) KO profiles. Only KO profiles related to energy
266 transduction oxidoreductases were used to search the genomes in this study, which were
267 extracted from Supplemental Table 1 in Jelen et al. (2016). Sequences were identified as positive
268 hits if their score was greater than or equal to 50% of the sequence threshold value as calculated
269 in KofamKOALA.

270

271 16S ribosomal RNA gene phylogeny

272 16S rRNA gene sequences predicted using cmsearch (Nawrocki and Eddy, 2013) were
273 filtered for sequences that were greater than or equal to 1200 bp using bioawk
274 (https://github.com/lh3/bioawk). Sequences that were 100% identical were removed using
275 dedupe.sh (https://github.com/BioInfoTools/BBMap). Sequences were then aligned using ssu-

276 align (Nawrocki, 2009), which produces two separate alignment files for Bacteria and Archaea.
277 Next, ambiguously aligned positions were removed using ssu-mask, and sequences were re-
278 checked to ensure that the masked alignment contained sequences that were greater than or equal
279 to 1200 bp. Sequences that did not meet these threshold requirements were removed from the
280 alignment file using ssu-mask with the "--seq-r" option and list of sequences to remove. The
281 Stockholm alignment file was converted to an aligned fasta file using ssu-mask with the "--
282 stk2afa" option. The masked and filtered alignment files for Bacteria and Archaea were used to
283 create phylogenetic trees using maximum likelihood reconstruction with FastTree (Price et al.,
284 2010) with the following parameters: "-nt -gtr -cat 20 -gamma". Both trees were visualized and
285 annotated using the Interactive Tree of Life (Letunic and Bork, 2019).
286
287 **Results and Discussion**
288
289 Global presence of Patescibacteria and DPANN in subsurface environments
290 To improve our understanding of the deep genealogy of Bacteria and Archaea, we
291 sequenced 4,829 single amplified genomes (SAGs; Table S1) of previously under-sampled
292 microbial lineages from 46 globally distributed field sites (Figure 1; Table S1). These sites were
293 chosen based on 16S rRNA gene amplicon screens that were enriched in bacterial and archaeal
294 candidate phyla. A maximum likelihood phylogenetic tree of concatenated single-copy proteins
295 (SCP) (Figure 2) positioned 22% and 4% of SAGs within Patescibacteria (n=492) and DPANN
296 archaea (n=81). The concatenated SCP phylogenetic tree revealed the separation of
297 Patescibacteria and DPANN from other Bacteria and Archaea, respectively, which corroborates
298 other phylogenetic reconstructions using diverse sets of single copy proteins and phylogenetic

tools (Rinke et al., 2013; Brown et al., 2015; Hug et al., 2016; Williams et al., 2017; Castelle et al., 2018; Dombrowski et al., 2019). Patescibacteria comprised a median relative abundance of 13% (range=0-81%) and DPANN comprised a median abundance of 7.5% (range=0-23%) in 33 analyzed environmental sites, with elevated abundances in deep-sourced aquifer environments (Figure 3). Most of the Patescibacteria and DPANN SAGs originated from 13 continental subsurface sites in Africa, Asia, and North America (Table S1). These results confirm that Patescibacteria and DPANN are globally abundant members of subsurface microbial communities, expanding on the prior genomic studies that were predominantly based on a small number of study locations in North America (Rinke et al., 2013; Luef et al., 2015; Castelle et al., 2018).

Evidence for physical cell-cell associations

We searched for evidence of physical cell-cell associations—an implication of obligate symbiosis—by identifying genomic sequences from multiple phylogenetically distinct organisms within individual SAGs. First, we searched for multiple copies of conserved, single copy protein-encoding genes using checkM (Parks et al., 2015), which is a commonly used tool to detect genome contamination. This approach identified 1% of Patescibacteria SAGs (5/492), 1.2% of DPANN SAGs (1/81), and 0.3% of SAGs from other phyla (5/1686) as containing DNA from heterogeneous sources (Table S3). Next, we searched for non-identical, near-full-length (> 1,000 bp) 16S rRNA genes in individual SAG assemblies. Such cases accounted for 1.5% of Patescibacteria (4/262), 0% DPANN (0/56), and 0.53% for other phyla (4/758) (Table S3). A Chi-square test revealed that there was a significant relationship between phyla and potential co-sorted SAGs from both checkM (p-value=1.2 x 10^{-13}; X^2=224.2) and 16S rRNA gene analyses

(p-value<2.2 x 10^{-16}; X^2=238.07), but the overall contribution of Patescibacteria and DPANN to the significance of co-sorted SAGs was very low (<0.5%) relative to other phyla (Figure 4). Due to the incomplete SAG assemblies (Table S1), these sequencing-based approaches may underestimate the overall frequency of cell-cell associations in our data set. However, they consistently show that putative cell-cell associations constitute only a minor fraction of all SAGs, and that Patescibacteria and DPANN are not significantly enriched in such associations relative to other phyla in the studied environments. Furthermore, all identified cases of heterogeneous DNA in SAG assemblies were phylogenetically unique (Table S3), in contrast to the recurring Nanoarchaeota-Crenarchaeota symbiotic associations found using the same techniques in hot springs in prior studies (Munson-McGee et al., 2015; Jarett et al., 2018). Also, in mammalian oral microbiomes, Saccharibacteria have been shown to be specifically associated with Actinobacteria hosts (He et al., 2015; Cross et al., 2019). This suggests that the infrequent and inconsistent presence of taxonomically heterogeneous DNA in SAGs most likely originated from non-specific aggregation of multiple cells and/or attachment of extracellular DNA.

Based on a small number of transmission electron micrograph observations, it has been suggested that Patescibacteria associations with other microorganisms may be fragile (Luef et al., 2015). Thus, we cannot rule out the possibility that some Patescibacteria and DPANN cells were attached to host cells *in situ* and became detached during sample collection and processing. To reduce the risk of dispersing natural cell aggregates and associations, we performed only a gentle mixing of the analyzed samples in preparation for cell sorting. In prior studies, similar techniques successfully revealed host-symbiont associations in termite guts (Hongoh et al., 2008), marine plankton (Martinez-Garcia et al., 2012) and hot springs (Jarett et al., 2018). This approach was also used to determine symbiotic associations between anaerobic methane-oxidizing archaea and

their syntrophic partners in natural consortia from methane seeps (Hatzenpichler et al., 2016). It is worthy to note that the Saccharibacteria-Actinobacteria symbiont-host relationship was only disrupted by physical passage through a narrow-gauge needle multiple times (He et al., 2015). Also, putatively co-sorted SAGs of Nanoarchaeota and Crenarchaeota from iron oxide microbial mats were treated by a repeated physical disruption through multiple wash cycles and density gradient centrifugation, from which co-sorted cells were obtained (Jarett et al., 2018). Thus, although the techniques applied here may underestimate the overall counts of cell-cell associations *in situ*, we found no evidence for Patescibacteria and DPANN to be enriched in such associations relative to other phyla, and to form lineage-specific associations in the analyzed environments.

Cell diameters

We employed calibrated index fluorescence-activated cell sorting (FACS) to determine physical diameters of individual cells that were used in SAG generation (Stepanauskas et al., 2017). This indicated that Patescibacteria (n=273) and DPANN (n=29) cells are extremely small across their entire phylogenetic breadth, with median estimated diameters of 0.2 μm (Figure 5). Several cases of larger, outlier diameter estimates may be due to attachment to other cells and particles, cellular division, methodological artifacts, or true biological variation. The low frequency of Patescibacteria and DPANN DNA recovery from larger particles (Table S1; Figure 5) provides further indication that most of these cells are not attached to other microorganisms. Likewise, most of the SAGs with identified heterogeneous genome sources were larger than their phylum median cell diameters (Table S3), which is consistent with their aggregation with other cells.

368 To further investigate the composition of extremely small cells, we generated a
369 complementary library of SAGs from a single subsurface sample (AG-274; Table S1) with a
370 FACS gate targeting only ≤0.3 µm particles. Confirming our expectations, >90% of SAGs in this
371 cell diameter-specific library were composed of Patescibacteria and DPANN (Figure 3). The
372 obtained cellular size ranges are consistent with a prior report, which was based on transmission
373 electron micrographs from one field study site (Luef et al., 2015). These cell diameters
374 approximate the lower theoretical limits for cellular life (Maniloff et al., 1997).
375
376 General genome features
377 To identify functional coding potential differences of Patescibacteria and DPANN
378 compared to other Bacteria and Archaea, we performed a principal component analysis (PCA)
379 using the relative abundance of clusters of orthologous groups (COG) as input variables with
380 SAGs that had at least 30% completeness and a near full-length 16S rRNA gene (Figure 6). This
381 showed a clear separation of Patescibacteria and DPANN from other bacteria and archaea along
382 the first component (PC1) (Wilcoxon signed-rank test; p-value < 2.2×10^{-16}). Importantly, well-
383 described symbionts (Table S4) separated from both Patescibacteria along PC1 and DPANN
384 along PC2 (p-value = 2.57×10^{-8} and 1.0×10^{-7} for Patescibacteria and DPANN, respectively).
385 The only lineages that clustered with Patescibacteria and DPANN along PC1 and PC2 were
386 Dependentiae and Tenericutes, respectively.
387 The COG categories with the greatest negative effect on PC1, indicative of their relative
388 depletion in Patescibacteria and DPANN, included E (amino acid metabolism and transport), C
389 (energy production and conversion), P (inorganic ion transport and metabolism), and H
390 (coenzyme transport and metabolism). The COG categories with the greatest positive effect on

PC1, indicative of their relatively high fraction in genomes of Patescibacteria and DPANN, included D (cell cycle control and mitosis) and O (post-translational modification, protein turnover, chaperone functions). Archaea separated from bacteria along the second component (PC2) (p-value < 2.2×10^{-16}) primarily by their relative enrichment in COG categories B (chromatin structure and dynamics), K (transcription), and S (unknown functions). This reflects the major inter-domain differences in DNA packing and transcription, and the greater fraction of archaeal genomes remaining uncharacterized, as compared to the genomes of Bacteria.

Genomes recently shaped by symbiosis often have low coding densities due to rapid gene loss and pseudogene formation (McCutcheon and Moran, 2012). Inconsistent with this pattern, we found the coding density of Patescibacteria and DPANN (median = 91%) to be typical of Bacteria and Archaea (median = 90%), while well-characterized symbionts were separated by their lower coding density (Figure 7a) (median = 0.87%, p-value = 0.035 and 0.028 compared to Patescibacteria and DPANN). Although the reduced genome size of Patescibacteria and DPANN has been viewed as an indication of a symbiotic lifestyle (Castelle et al., 2018), similar genome sizes (1-2 Mbp) are typical among free-living, marine plankton (Swan et al., 2013; Giovannoni et al., 2014). Furthermore, recent synthetic biology experimentation has pushed the minimal genome size limit of a free-living microorganism to ~0.5 Mbp (Hutchison et al., 2016), far below the predicted sizes of Patescibacteria and DPANN genomes. Collectively, these general genome features of Patescibacteria and DPANN do not provide convincing evidence of an obligate symbiotic lifestyle.

In this context, the observed gene content similarities between Patescibacteria and Dependentiae, and between DPANN and most Tenericutes are intriguing (Figure 6). Dependentiae is a candidate bacterial phylum that has been noted for its reduced coding

potential, including a depletion in electron transport chain components (McLean et al., 2013; Yeoh et al., 2016). It has been speculated that these characteristics indicate a symbiotic lifestyle, with energy acquired from hosts via ATP/ADP translocases, which has been confirmed experimentally in a few Dependentiae members (Delafont et al., 2015; Pagnier et al., 2015; Deeg et al., 2019). The well-characterized members of the bacterial phylum Tenericutes consist mostly of obligate pathogens with reduced genomes (Moran and Wernegreen, 2000). Interestingly, most Tenericutes are able to grow as free-living cells in rich media solely by fermentation (Tully et al., 1977), and were originally hypothesized to represent ancient lineages of life due to their small genome sizes and limited metabolisms (Morowitz, 1984). While we found all analyzed Dependentiae and most Tenericutes deplete in oxidoreductases (Figures 7b; Figure 8), only Tenericutes had a consistently low coding density (median = 71%) that is a characteristic of recently evolved symbionts (McCutcheon and Moran, 2012) (Figure 7a). Thus, we hypothesize that these two phyla cluster with the Patescibacteria and DPANN due to similar metabolic features arrived at by convergent evolutionary processes.

Oxygen reductase genes

In search for an alternative explanation for the unique genealogy, genome content, and cell sizes of Patescibacteria and DPANN, we examined their energy metabolic coding potential. We found that only 0.6% of Patescibacteria SAGs (3/492) and none of the DPANN SAGs (0/81) from these samples encoded for homologs of oxygen reductases (O_2red), as indicated by the presence of oxygen-binding subunit I of either the heme-copper oxidase (HCO) or bd-ubiquinol (bd) oxidase families. The incomplete genome recovery from individual SAGs cannot explain this pattern, because the 492 Patescibacteria SAGs and 81 DPANN SAGs correspond to a

cumulative assembly of 162 and 27 randomly sampled, complete genomes. Furthermore, a phylogenetic analysis revealed that all three oxygen reductases from Patescibacteria SAGs form a cluster with other Patescibacteria sequences (Brown et al., 2015; Nelson and Stegen, 2015; León-Zayas et al., 2017) that is nested within a clade comprised of other phyla (Figure 9). We infer these phylogenetic relationships as an indication of a relatively recent horizontal gene transfer (HGT), likely from Proteobacteria and Firmicutes for the HCO and bd sequences, respectively. Although we did not detect any homologs of oxygen reductases in DPANN SAGs from our samples, the publicly available bd O_2red sequences from DPANN metagenome bins and isolates formed a clade with Actinobacteria and Firmicutes, which we also infer as likely products of relatively recent HGT events. The topology of these O_2red phylogenetic trees is consistent with prior reports, which have also been interpreted as evidence for prevalent HGT of oxygen reductase genes among other phyla (Brochier-Armanet et al., 2009; Gribaldo et al., 2009; Borisov et al., 2011). This suggests that the absence of oxygen reductases in Patescibacteria and DPANN is ancestral and not a result of gene loss due to adaptations to symbiosis, as previously hypothesized (Castelle et al., 2018).

Distribution of electron transport chain complexes

Patescibacteria and DPANN were depleted in the entire family of oxidoreductase enzyme genes compared to other bacteria and archaea, (p-value $< 2.2 \times 10^{-16}$) (Figures 7b, 8). This depletion was also significant in relation to symbionts with their comparatively small genome sizes (p-value < 0.05). Oxidoreductases are key components of both aerobic and anaerobic respiratory pathways (Jelen et al., 2016), so underrepresentation of them would suggest reduced functionality of these energy transduction mechanisms. Accordingly, none of the Patescibacteria

and DPANN genomes were found to encode a complete ETC consisting of all four complexes (Figure 8). Putative homologs of at least two of the four ETC complexes were found only in 3% and 11% of Patescibacteria and DPANN genomes, respectively. We found putative homologs of genes encoding individual complexes I, II, III, and IV in 0%, 2%, 3%, and 14% of Patescibacteria genomes. The corresponding numbers for DPANN were 7%, 4%, 0%, and 21%. Some of these computationally predicted genes are only distantly related to experimentally verified homologs and therefore may constitute false positives. These findings are consistent with the lack of complete ETC reports in prior studies of Patescibacteria genomes (Brown et al., 2015), with the sole exception of a tentative nitric oxide respiration operon found in a single metagenome bin (Castelle et al., 2017). The sparse and scattered distribution of the putative ETC gene homologs in Patescibacteria and DPANN (Figure 8) suggest horizontal gene transfer origins rather than ancestral inheritance. This is consistent with the phylogenetic reconstructions of other energy transducing genes identified in Patescibacteria, which also suggest evolutionary origins from horizontal gene transfer (Jaffe et al., 2019). Collectively, our observations indicate that the absence of complete electron transport chains in Patescibacteria and DPANN is an ancestral feature, which we propose is more parsimonious than multiple gene loss events due to obligate symbiosis (Brown et al., 2015; Hug et al., 2016; Castelle et al., 2018; Dombrowski et al., 2019; Méheust et al., 2019).

Respiration activity

To experimentally test for the presence of active oxidoreductases in a subsurface microbial community, we employed the fluorogenic oxidoreductase probe RedoxSensor Green on a deep groundwater sample from South Dakota. This revealed a wide range in fluorescence

intensity in phylogenetically diverse cells, with none of the Patescibacteria cells exceeding the fluorescence of particles in a heat-killed, negative control (Figure 10). To the best of our knowledge, RedoxSensor Green has not been tested extensively on diverse microbial lineages, therefore these results should be considered tentative. Nonetheless, both genome content and *in situ* physiology analyses indicate the absence of respiration in Patescibacteria and DPANN, which corroborates earlier reports of these lineages containing few, if any, components of energy transducing pathways other than fermentation (Castelle et al., 2018).

16S rRNA gene phylogeny

The placement of Patescibacteria and DPANN in the tree of life is widely debated (Hug et al., 2016; Williams et al., 2017; Dombrowski et al., 2019). Most current phylogenetic inferences are based on concatenated single-copy proteins (CSCP), which has the advantage of higher phylogenetic resolution, as compared to phylogenies of individual genes (Rinke et al., 2013). However, the unknown genetic change at heterogeneously evolving sites and large sequence divergence may limit the accuracy of such trees (Pace, 2009; Dombrowski et al., 2019). To complement the CSCP-resolved genealogy (Figure 2), we performed a large-scale phylogenetic analysis of the well-established 16S rRNA gene (Woese, 2002) (length > 1,200 bp) separately for Bacteria and Archaea. The obtained phylogenetic inference (Figure 8) supported the separation of Patescibacteria and DPANN from other bacterial and archaeal lineages, in agreement with the phylogenies based on CSCP genes (Castelle et al., 2018) (Figure 2) and a recent large scale bacterial 16S rRNA gene tree (Schulz et al., 2017). Importantly, we did not observe grouping of Patescibacteria with fast-evolving lineages (e.g., obligate insect symbionts and Tenericutes) that could be due to long branch attraction in the 16S rRNA gene phylogeny.

506 This suggests that the divergent branching of Patescibacteria and DPANN is probably not a
507 result of recent, accelerated divergence.
508
509 **Concluding Remarks**
510 Using the collective evidence from cell-cell association, coding potential and
511 phylogenomic analyses, we propose a new explanation of the unusual biological features of
512 Patescibacteria and DPANN. Although the Patescibacteria and DPANN contain symbionts
513 (Huber et al., 2002; Podar et al., 2013; Gong et al., 2014; He et al., 2015; Munson-McGee et al.,
514 2015; Jarett et al., 2018; Cross et al., 2019; Hamm et al., 2019) and auxotrophies (Castelle et al.,
515 2018; Dombrowski et al., 2019), we believe that there is not sufficient evidence to conclude that
516 an ancestral adaptation to symbiosis has led to the reduction of their cell sizes and coding
517 potential (Castelle et al., 2018; Dombrowski et al., 2019; Méheust et al., 2019). Instead, our data
518 indicate that most Patescibacteria and DPANN do not form symbiotic cell-cell associations in
519 subsurface environments, and that their divergent coding potential, small genomes, and small
520 cell sizes may be a result of a primitive energy metabolism that relies solely on substrate-level
521 phosphorylation (fermentation), potentially preceding the evolution of electron transport
522 phosphorylation (respiration). Auxotrophies are very common among microorganisms, and
523 represent a wide range of dependencies for exogenous cellular components (Zengler and
524 Zaramela, 2018). Patescibacteria and DPANN may be on the extreme end of the spectrum in
525 their dependence on other community members, perhaps a reflection of an ancient evolutionary
526 strategy to limit cellular biosynthetic energy requirements, as energetic allocation is a major
527 driver of genome evolution in bacteria and archaea (Lynch and Marinov, 2015).
528

529 The authors declare no conflict of interest.

530

531 **Acknowledgements**

532

533 We thank the staff of the Bigelow Laboratory for Ocean Science Single Cell Genomics Center
534 (SCGC) for the generation of single cell genomic data. We also thank Paul Falkowski and Saroj
535 Poudel for advice on electron transport systems, Jacob Munson-McGee for insightful discussions
536 on co-sorted SAGs, and David Emerson, Sean Crowe, Paul van der Wielen, Sari Peura, Andreas
537 Teske, Takuro Nunoura, Christa Schleper, and Steffen Joergensen for contributing field samples.
538 Thanks also to Richard Friese, Josh Hoines, and Kevin Wilson (National Park Service); Michael
539 King and John Bredehoft (Hydrodynamics Group); Darrell Lacy, Levi Kryder, John Klenke, and
540 Jamie Walker (Nuclear Waste Repository Project Office); and Jaret Heise, Tom Regan and
541 others at Sanford Underground Research Facility (SURF); Corey Lee (US Fish and Wildlife
542 Service) and The Nature Conservancy for site access and sampling assistance in Nevada and
543 South Dakota. Special thanks to Brittany Kruger, Josh Sackett, Scott Hamilton-Brehm, John
544 Healey, Brad Lyles, and Chuck Russell of DRI for sampling assistance in Nevada. Thanks to the
545 U.S. Forest Service for a permit to conduct research at Little Hot Creek, California and the 2015
546 International Geobiology Course for field work and sample collection. We also thank Vitaly
547 Kadnikov, Olga Karnachuk and Tamara Zemskaya for sample collection in Siberia. Also, thanks
548 to Stephen Grasby, Allyson Brady, and Christine Sharp for sampling Canadian field samples,
549 and Wen-Jun Li for logistical support and access to hot spring samples in China. We also thank
550 British Columbia Parks and Parks Canada for permission to sample Dewar Creek and Paint Pots
551 field sites. This work was funded by the USA National Science Foundation grants 1441717,

552 1826734, and 1335810 (to RS); and 1460861 (REU site at Bigelow Laboratory for Ocean
553 Sciences). TW, FS and JJ were funded by the U.S. Department of Energy Joint Genome Institute,
554 a DOE Office of Science User Facility supported under Contract No. DE-AC02-05CH11231.
555 NVR group was funded by the Russian Science Foundation (grant 19-14-00245). SMS was
556 funded by USA National Science Foundation grants OCE-0452333 and OCE-1136727. BPH was
557 funded by NASA Exobiology grant 80NSSC17K0548.
558

559 **Author contributions**

560 JPB led data analyses and manuscript preparation. RS developed the concept and managed the
561 project, with contributions by TW, TCO, DM, JAE, JPB and EDB. EDB, JMB, FS, JKJ, OB, KC
562 contributed to data analyses. NJP performed cell sorting and size calibration at Bigelow
563 Laboratory. TCO, DPM, PD, NVR, JRS, BPH, KAK, SMS, MSE, HAB and MBS oversaw field
564 sample collection. All authors contributed to data interpretation and manuscript preparation.
565

566 **References**

567 Altschul, S. F., Gish, W., Miller, W., Myers, E. W., and Lipman, D. J. (1990). Basic local
568 alignment search tool. *J. Mol. Biol.* 215, 403–410. doi:10.1016/S0022-2836(05)80360-2.
569 Altschul, S. F., Madden, T. L., Schäffer, A. A., Zhang, J., Zhang, Z., Miller, W., et al. (1997).
570 Gapped BLAST and PSI-BLAST: A new generation of protein database search programs.
571 *Nucleic Acids Res.* 25, 3389–3402. doi:10.1093/nar/25.17.3389.
572 Aramaki, T., Blanc-Mathieu, R., Endo, H., Ohkubo, K., Kanehisa, M., Goto, S., et al. (2019).
573 KofamKOALA: KEGG ortholog assignment based on profile HMM and adaptive score
574 threshold. *bioRxiv*, 602110. doi:10.1101/602110.

575 Bankevich, A., Nurk, S., Antipov, D., Gurevich, A. A., Dvorkin, M., Kulikov, A. S., et al.
576 (2012). SPAdes: A new genome assembly algorithm and its applications to single-cell
577 sequencing. *J. Comput. Biol.* 19, 455–477. doi:10.1089/cmb.2012.0021.
578 Bateman, A., Martin, M. J., O'Donovan, C., Magrane, M., Alpi, E., Antunes, R., et al. (2017).
579 UniProt: The universal protein knowledgebase. *Nucleic Acids Res.* 45, D158–D169.
580 doi:10.1093/nar/gkw1099.
581 Becraft, E. D., Woyke, T., Jarett, J., Ivanova, N., Godoy-Vitorino, F., Poulton, N., et al. (2017).
582 Rokubacteria: Genomic giants among the uncultured bacterial phyla. *Front. Microbiol.* 8,
583 1–12. doi:10.3389/fmicb.2017.02264.
584 Borisov, V. B., Gennis, R. B., Hemp, J., and Verkhovsky, M. I. (2011). The cytochrome bd
585 respiratory oxygen reductases. *Biochim. Biophys. Acta - Bioenerg.* 1807, 1398–1413.
586 doi:10.1016/j.bbabio.2011.06.016.
587 Brochier-Armanet, C., Talla, E., and Gribaldo, S. (2009). The multiple evolutionary histories of
588 dioxygen reductases: Implications for the origin and evolution of aerobic respiration. *Mol.*
589 *Biol. Evol.* 26, 285–297. doi:10.1093/molbev/msn246.
590 Brown, C. T., Hug, L. A., Thomas, B. C., Sharon, I., Castelle, C. J., Singh, A., et al. (2015).
591 Unusual biology across a group comprising more than 15% of domain Bacteria. *Nature* 523,
592 208–211. doi:10.1038/nature14486.
593 Brown, C. T., Olm, M. R., Thomas, B. C., and Banfield, J. F. (2016). Measurement of bacterial
594 replication rates in microbial communities. *Nat. Biotechnol.* 34, 1256–1263.
595 doi:10.1038/nbt.3704.
596 Capella-Gutiérrez, S., Silla-Martínez, J. M., and Gabaldón, T. (2009). trimAl: A tool for
597 automated alignment trimming in large-scale phylogenetic analyses. *Bioinformatics* 25,

1972–1973. doi:10.1093/bioinformatics/btp348.

Castelle, C. J., and Banfield, J. F. (2018). Major New Microbial Groups Expand Diversity and Alter our Understanding of the Tree of Life. *Cell* 172, 1181–1197. doi:10.1016/j.cell.2018.02.016.

Castelle, C. J., Brown, C. T., Anantharaman, K., Probst, A. J., Huang, R. H., and Banfield, J. F. (2018). Biosynthetic capacity, metabolic variety and unusual biology in the CPR and DPANN radiations. *Nat. Rev. Microbiol.* 16, 629–645. doi:10.1038/s41579-018-0076-2.

Castelle, C. J., Brown, C. T., Thomas, B. C., Williams, K. H., and Banfield, J. F. (2017). Unusual respiratory capacity and nitrogen metabolism in a Parcubacterium (OD1) of the Candidate Phyla Radiation. *Sci. Rep.* 7, 1–12. doi:10.1038/srep40101.

Castelle, C. J., Wrighton, K. C., Thomas, B. C., Hug, L. A., Brown, C. T., Wilkins, M. J., et al. (2015). Genomic expansion of domain archaea highlights roles for organisms from new phyla in anaerobic carbon cycling. *Curr. Biol.* 25, 690–701. doi:10.1016/j.cub.2015.01.014.

Chen, I. M. A., Chu, K., Palaniappan, K., Pillay, M., Ratner, A., Huang, J., et al. (2019). IMG/M v.5.0: An integrated data management and comparative analysis system for microbial genomes and microbiomes. *Nucleic Acids Res.* 47, D666–D677. doi:10.1093/nar/gky901.

Criscuolo, A., and Gribaldo, S. (2010). BMGE (Block Mapping and Gathering with Entropy): A new software for selection of phylogenetic informative regions from multiple sequence alignments. *BMC Evol. Biol.* 10. doi:10.1186/1471-2148-10-210.

Cross, K. L., Campbell, J. H., Balachandran, M., Campbell, A. G., Cooper, S. J., Griffen, A., et al. (2019). Targeted isolation and cultivation of uncultivated bacteria by reverse genomics. *Nat. Biotechnol.* doi:10.1038/s41587-019-0260-6.

Deeg, C. M., Zimmer, M. M., George, E. E., Husnik, F., Keeling, P. J., and Suttle, C. A. (2019).

621 Chromulinavorax destructans, a pathogen of microzooplankton that provides a window into
622 the enigmatic candidate phylum dependentiae. *PLoS Pathog.* 15, 1–18.
623 doi:10.1371/journal.ppat.1007801.
624 Delafont, V., Samba-Louaka, A., Bouchon, D., Moulin, L., and Héchard, Y. (2015). Shedding
625 light on microbial dark matter: A TM6 bacterium as natural endosymbiont of a free-living
626 amoeba. *Environ. Microbiol. Rep.* 7, 970–978. doi:10.1111/1758-2229.12343.
627 Dombrowski, N., Lee, J. H., Williams, T. A., Offre, P., and Spang, A. (2019). Genomic
628 diversity, lifestyles and evolutionary origins of DPANN archaea. *FEMS Microbiol. Lett.*
629 366, 1–12. doi:10.1093/femsle/fnz008.
630 Eddy, S. R. (2011). Accelerated profile HMM searches. *PLoS Comput. Biol.* 7.
631 doi:10.1371/journal.pcbi.1002195.
632 Eloe-Fadrosh, E. A., Paez-Espino, D., Jarett, J., Dunfield, P. F., Hedlund, B. P., Dekas, A. E., et
633 al. (2016). Global metagenomic survey reveals a new bacterial candidate phylum in
634 geothermal springs. *Nat. Commun.* 7, 1–10. doi:10.1038/ncomms10476.
635 Giovannoni, S. J., Cameron Thrash, J., and Temperton, B. (2014). Implications of streamlining
636 theory for microbial ecology. *ISME J.* 8, 1553–1565. doi:10.1038/ismej.2014.60.
637 Gong, J., Qing, Y., Guo, X., and Warren, A. (2014). “Candidatus Sonnebornia yantaiensis”, a
638 member of candidate division OD1, as intracellular bacteria of the ciliated protist
639 Paramecium bursaria (Ciliophora, Oligohymenophorea). *Syst. Appl. Microbiol.* 37, 35–41.
640 doi:10.1016/j.syapm.2013.08.007.
641 Gribaldo, S., Talla, E., and Brochier-Armanet, C. (2009). Evolution of the haem copper oxidases
642 superfamily: a rooting tale. *Trends Biochem. Sci.* 34, 375–381.
643 doi:10.1016/j.tibs.2009.04.002.

644 Hamm, J. N., Erdmann, S., Eloe-Fadrosh, E. A., Angeloni, A., Zhong, L., Brownlee, C., et al.
645 (2019). Unexpected host dependency of Antarctic Nanohaloarchaeota. *Proc. Natl. Acad.*
646 *Sci. U. S. A.* 116, 14661–14670. doi:10.1073/pnas.1905179116.
647 Hatzenpichler, R., Connon, S. A., Goudeau, D., Malmstrom, R. R., Woyke, T., and Orphan, V. J.
648 (2016). Visualizing in situ translational activity for identifying and sorting slow-growing
649 archaeal - bacterial consortia. *Proc. Natl. Acad. Sci. U. S. A.* 113, E4069–E4078.
650 doi:10.1073/pnas.1603757113.
651 He, X., McLean, J. S., Edlund, A., Yooseph, S., Hall, A. P., Liu, S. Y., et al. (2015). Cultivation
652 of a human-associated TM7 phylotype reveals a reduced genome and epibiotic parasitic
653 lifestyle. *Proc. Natl. Acad. Sci. U. S. A.* 112, 244–249. doi:10.1073/pnas.1419038112.
654 Hershey, O. S., Kallmeyer, J., Wallace, A., Barton, M. D., and Barton, H. A. (2018). High
655 microbial diversity despite extremely low biomass in a deep karst aquifer. *Front. Microbiol.*
656 9, 1–13. doi:10.3389/fmicb.2018.02823.
657 Hongoh, Y., Sharma, V. K., Prakash, T., Noda, S., Taylor, T. D., Kudo, T., et al. (2008).
658 Complete genome of the uncultured Termite Group 1 bacteria in a single host protist cell.
659 *Proc. Natl. Acad. Sci. U. S. A.* 105, 5555–5560. doi:10.1073/pnas.0801389105.
660 Huber, H., Hohn, M. J., Rachel, R., Fuchs, T., Wimmer, V. C., and Stetter, K. O. (2002). A new
661 phylum of Archaea represented by a nanosized hyperthermophilic symbiont. *Nature* 417,
662 63–67. doi:10.1038/417063a.
663 Hug, L. A., Baker, B. J., Anantharaman, K., Brown, C. T., Probst, A. J., Castelle, C. J., et al.
664 (2016). A new view of the tree of life. *Nat. Microbiol.* 1, 1–6.
665 doi:10.1038/nmicrobiol.2016.48.
666 Huntemann, M., Ivanova, N. N., Mavromatis, K., Tripp, H. J., Paez-Espino, D., Tennessen, K., et

667 al. (2016). The standard operating procedure of the DOE-JGI Metagenome Annotation
668 Pipeline (MAP v.4). *Stand. Genomic Sci.* 11, 1–5. doi:10.1186/s40793-016-0138-x.
669 Hutchison, C. A., Chuang, R. Y., Noskov, V. N., Assad-Garcia, N., Deerinck, T. J., Ellisman, M.
670 H., et al. (2016). Design and synthesis of a minimal bacterial genome. *Science (80-.).* 351.
671 doi:10.1126/science.aad6253.
672 Hyatt, D., Chen, G. L., LoCascio, P. F., Land, M. L., Larimer, F. W., and Hauser, L. J. (2010).
673 Prodigal: Prokaryotic gene recognition and translation initiation site identification. *BMC*
674 *Bioinformatics* 11. doi:10.1186/1471-2105-11-119.
675 Jaffe, A. L., Castelle, C. J., Carnevali, P. B. M., Gribaldo, S., and Banfield, J. F. (2019). The rise
676 of diversity in metabolic platforms across the Candidate Phyla Radiation. *bioRxiv*, 1–29.
677 Jain, C., Rodriguez-R, L. M., Phillippy, A. M., Konstantinidis, K. T., and Aluru, S. (2018). High
678 throughput ANI analysis of 90K prokaryotic genomes reveals clear species boundaries. *Nat.*
679 *Commun.* 9, 1–8. doi:10.1038/s41467-018-07641-9.
680 Jarett, J. K., Nayfach, S., Podar, M., Inskeep, W., Ivanova, N. N., Munson-Mcgee, J., et al.
681 (2018). Single-cell genomics of co-sorted Nanoarchaeota suggests novel putative host
682 associations and diversification of proteins involved in symbiosis 06 Biological Sciences
683 0604 Genetics. *Microbiome* 6, 1–14. doi:10.1186/s40168-018-0539-8.
684 Jelen, B. I., Giovannelli, D., and Falkowski, P. G. (2016). The Role of Microbial Electron
685 Transfer in the Coevolution of the Biosphere and Geosphere. *Annu. Rev. Microbiol.* 70, 45–
686 62. doi:10.1146/annurev-micro-102215-095521.
687 León-Zayas, R., Peoples, L., Biddle, J. F., Podell, S., Novotny, M., Cameron, J., et al. (2017).
688 The metabolic potential of the single cell genomes obtained from the Challenger Deep,
689 Mariana Trench within the candidate superphylum Parcubacteria (OD1). *Environ.*

690 *Microbiol.* 19, 2769–2784. doi:10.1111/1462-2920.13789.

691 Letunic, I., and Bork, P. (2019). Interactive Tree Of Life (iTOL) v4: recent updates and new

692 developments. *Nucleic Acids Res.* 47, W256–W259. doi:10.1093/nar/gkz239.

693 Luef, B., Frischkorn, K. R., Wrighton, K. C., Holman, H. Y. N., Birarda, G., Thomas, B. C., et

694 al. (2015). Diverse uncultivated ultra-small bacterial cells in groundwater. *Nat. Commun.* 6,

695 1–8. doi:10.1038/ncomms7372.

696 Lynch, M., and Marinov, G. K. (2015). The bioenergetic costs of a gene. *Proc. Natl. Acad. Sci.*

697 *U. S. A.* 112, 15690–15695. doi:10.1073/pnas.1514974112.

698 Maniloff, J., Nealson, K. H., Psenner, R., Loferer, M., and Folk, R. L. (1997). Nannobacteria:

699 Size Limits and Evidence. *Science (80-.).* 276, 1773–1776.

700 Martinez-Garcia, M., Brazel, D., Poulton, N. J., Swan, B. K., Gomez, M. L., Masland, D., et al.

701 (2012). Unveiling in situ interactions between marine protists and bacteria through single

702 cell sequencing. *ISME J.* 6, 703–707. doi:10.1038/ismej.2011.126.

703 McCutcheon, J. P., and Moran, N. A. (2012). Extreme genome reduction in symbiotic bacteria.

704 *Nat. Rev. Microbiol.* 10, 13–26. doi:10.1038/nrmicro2670.

705 McLean, J. S., Lombardo, M. J., Badger, J. H., Edlund, A., Novotny, M., Yee-Greenbaum, J., et

706 al. (2013). Candidate phylum TM6 genome recovered from a hospital sink biofilm provides

707 genomic insights into this uncultivated phylum. *Proc. Natl. Acad. Sci. U. S. A.* 110.

708 doi:10.1073/pnas.1219809110.

709 Méheust, R., Burstein, D., Castelle, C. J., and Banfield, J. F. (2019). The distinction of CPR

710 bacteria from other bacteria based on protein family content. *Nat. Commun.* 10.

711 doi:10.1038/s41467-019-12171-z.

712 Moran, N. A., and Wernegreen, J. J. (2000). Lifestyle evolution in symbiotic bacteria: Insights

713 from genomics. *Trends Ecol. Evol.* 15, 321–326. doi:10.1016/S0169-5347(00)01902-9.

714 Morowitz, H. (1984). The Completeness of Molecular Biology. *Isr. J. Med. Sci.* 20, 750–753.

715 Moser, D. P., Hamilton-Brehm, S. D., Fisher, J. C., Bruckner, J. C., Kruger, B., and Sackett, J.

716 (2015). Radiochemically-supported microbial communities: a potential mechanism for

717 biocolloid production of importance to actinide transport.

718 Munson-McGee, J. H., Field, E. K., Bateson, M., Rooney, C., Stepanauskas, R., and Young, J.

719 (2015). Distribution across Yellowstone National Park Hot Springs. *Appl. Environ.*

720 *Microbiol.* 81, 7860–7868. doi:10.1128/AEM.01539-15.Editor.

721 Nakamura, T., Yamada, K. D., Tomii, K., and Katoh, K. (2018). Parallelization of MAFFT for

722 large-scale multiple sequence alignments. *Bioinformatics* 34, 2490–2492.

723 doi:10.1093/bioinformatics/bty121.

724 Nawrocki, E. P. (2009). Structural RNA Homology Search and Alignment Using Covariance

725 Models.

726 Nawrocki, E. P., and Eddy, S. R. (2013). Infernal 1.1: 100-fold faster RNA homology searches.

727 *Bioinformatics* 29, 2933–2935. doi:10.1093/bioinformatics/btt509.

728 Nelson, W. C., and Stegen, J. C. (2015). The reduced genomes of Parcubacteria (OD1) contain

729 signatures of a symbiotic lifestyle. *Front. Microbiol.* 6, 1–14.

730 doi:10.3389/fmicb.2015.00713.

731 Nurk, S., Bankevich, A., Antipov, D., Gurevich, A. A., Korobeynikov, A., Lapidus, A., et al.

732 (2013). Assembling single-cell genomes and mini-metagenomes from chimeric MDA

733 products. *J. Comput. Biol.* 20, 714–737. doi:10.1089/cmb.2013.0084.

734 Pace, N. R. (2009). Mapping the Tree of Life: Progress and Prospects. *Microbiol. Mol. Biol. Rev.*

735 73, 565–576. doi:10.1128/mmbr.00033-09.

736 Pagnier, I., Yutin, N., Croce, O., Makarova, K. S., Wolf, Y. I., Benamar, S., et al. (2015). Babela
737 massiliensis, a representative of a widespread bacterial phylum with unusual adaptations to
738 parasitism in amoebae. *Biol. Direct* 10, 1–17. doi:10.1186/s13062-015-0043-z.
739 Parks, D. H., Imelfort, M., Skennerton, C. T., Hugenholtz, P., and Tyson, G. W. (2015).
740 CheckM: Assessing the quality of microbial genomes recovered from isolates, single cells,
741 and metagenomes. *Genome Res.* 25, 1043–1055. doi:10.1101/gr.186072.114.
742 Podar, M., Makarova, K. S., Graham, D. E., Wolf, Y. I., Koonin, E. V., and Reysenbach, A. L.
743 (2013). Insights into archaeal evolution and symbiosis from the genomes of a nanoarchaeon
744 and its inferred crenarchaeal host from Obsidian Pool, Yellowstone National Park. *Biol.*
745 *Direct* 8, 1–20. doi:10.1186/1745-6150-8-9.
746 Price, M. N., Dehal, P. S., and Arkin, A. P. (2010). FastTree 2 - Approximately maximum-
747 likelihood trees for large alignments. *PLoS One* 5. doi:10.1371/journal.pone.0009490.
748 Quast, C., Pruesse, E., Yilmaz, P., Gerken, J., Schweer, T., Yarza, P., et al. (2013). The SILVA
749 ribosomal RNA gene database project: Improved data processing and web-based tools.
750 *Nucleic Acids Res.* 41, 590–596. doi:10.1093/nar/gks1219.
751 Rinke, C., Schwientek, P., Sczyrba, A., Ivanova, N. N., Anderson, I. J., Cheng, J. F., et al.
752 (2013). Insights into the phylogeny and coding potential of microbial dark matter. *Nature*
753 499, 431–437. doi:10.1038/nature12352.
754 Sackett, J. D. (2018). Prokaryotic diversity and aqueous geochemistry of subsurface
755 environments of the Death Valley Regional Flow System.
756 Sackett, J. D., Huerta, D. C., Kruger, B. R., Hamilton-Brehm, S. D., and Moser, D. P. (2018). A
757 comparative study of prokaryotic diversity and physicochemical characteristics of devils
758 hole and the ash meadows fish conservation facility, a constructed analog. *PLoS One* 13, 1–

21. doi:10.1371/journal.pone.0194404.

Sackett, J. D., Kruger, B. R., Becraft, E. D., Jarett, J. K., Stepanauskas, R., Woyke, T., et al. (2019). Four Draft Single-Cell Genome Sequences of Novel, Nearly Identical Kiritimatiellaeota Strains Isolated from the Continental Deep Subsurface . *Microbiol. Resour. Announc.* 8, 1–4. doi:10.1128/mra.01249-18.

Safarian, S., Rajendran, C., Müller, H., Preu, J., Langer, J. D., Ovchinnikov, S., et al. (2016). Structure of a bd oxidase indicates similar mechanisms for membraneintegrated oxygen reductases. *Science (80-.).* 352, 583–586. doi:10.1126/science.aaf2477.

Schloss, P. D., Westcott, S. L., Ryabin, T., Hall, J. R., Hartmann, M., Hollister, E. B., et al. (2009). Introducing mothur: Open-source, platform-independent, community-supported software for describing and comparing microbial communities. *Appl. Environ. Microbiol.* 75, 7537–7541. doi:10.1128/AEM.01541-09.

Schulz, F., Eloe-Fadrosh, E. A., Bowers, R. M., Jarett, J., Nielsen, T., Ivanova, N. N., et al. (2017). Towards a balanced view of the bacterial tree of life. *Microbiome* 5, 140. doi:10.1186/s40168-017-0360-9.

Seemann, T. (2014). Prokka: Rapid prokaryotic genome annotation. *Bioinformatics* 30, 2068–2069. doi:10.1093/bioinformatics/btu153.

Shen, W., Le, S., Li, Y., and Hu, F. (2016). SeqKit: A cross-platform and ultrafast toolkit for FASTA/Q file manipulation. *PLoS One* 11, 1–10. doi:10.1371/journal.pone.0163962.

Sousa, F. L., Alves, R. J., Pereira-Leal, J. B., Teixeira, M., and Pereira, M. M. (2011). A bioinformatics classifier and database for Heme-Copper oxygen reductases. *PLoS One* 6, 1–9. doi:10.1371/journal.pone.0019117.

Stepanauskas, R., Fergusson, E. A., Brown, J., Poulton, N. J., Tupper, B., Labonté, J. M., et al.

(2017). Improved genome recovery and integrated cell-size analyses of individual uncultured microbial cells and viral particles. *Nat. Commun.* 8. doi:10.1038/s41467-017-00128-z.

Swan, B. K., Tupper, B., Sczyrba, A., Lauro, F. M., Martinez-Garcia, M., Gonźalez, J. M., et al. (2013). Prevalent genome streamlining and latitudinal divergence of planktonic bacteria in the surface ocean. *Proc. Natl. Acad. Sci. U. S. A.* 110, 11463–11468. doi:10.1073/pnas.1304246110.

Team, Rs. (2016). RStudio: Integrated Development for R.

Thomas, J. M., Moser, D. P., Fisher, J. C., Reihle, J., Wheatley, A., Hershey, R. L., et al. (2013). Using Water Chemistry, Isotopes and Microbiology to Evaluate Groundwater Sources, Flow Paths and Geochemical Reactions in the Death Valley Flow System, USA. *Procedia Earth Planet. Sci.* 7, 842–845. doi:10.1016/j.proeps.2013.03.033.

Tully, J. G., Whitcomb, R. F., Clark, F. H., and Williamson, D. L. (1977). Pathogenic mycoplasmas: Cultivation and vertebrate pathogenicity of a new spiroplasma. *Science (80-.).* 195, 892–894. doi:10.1126/science.841314.

Wickham, H. (2016). ggplot2: Elegant Graphics for Data Analysis. Available at: https://ggplot2.tidyverse.org.

Williams, T. A., Szöllosi, G. J., Spang, A., Foster, P. G., Heaps, S. E., Boussau, B., et al. (2017). Integrative modeling of gene and genome evolution roots the archaeal tree of life. *Proc. Natl. Acad. Sci. U. S. A.* 114, E4602–E4611. doi:10.1073/pnas.1618463114.

Woese, C. R. (2002). On the evolution of cells. *Proc. Natl. Acad. Sci. U. S. A.* 99, 8742–8747. doi:10.1073/pnas.132266999.

Woyke, T., Xie, G., Copeland, A., González, J. M., Han, C., Kiss, H., et al. (2009). Assembling

805 the marine metagenome, one cell at a time. *PLoS One* 4. doi:10.1371/journal.pone.0005299.

806 Wrighton, K. C., Thomas, B. C., Sharon, I., Miller, C. S., Castelle, C. J., VerBerkmoes, N. C., et

807 al. (2012). Fermentation, hydrogen, and sulfur metabolism in multiple uncultivated bacterial

808 phyla. *Science (80-.).* 337, 1661–1665. doi:10.1126/science.1224041.

809 Yeoh, Y. K., Sekiguchi, Y., Parks, D. H., and Hugenholtz, P. (2016). Comparative genomics of

810 candidate phylum tm6 suggests that parasitism is widespread and ancestral in this lineage.

811 *Mol. Biol. Evol.* 33, 915–927. doi:10.1093/molbev/msv281.

812 Yu, F. B., Blainey, P. C., Schulz, F., Woyke, T., Horowitz, M. A., and Quake, S. R. (2017).

813 Microfluidic-based mini-metagenomics enables discovery of novel microbial lineages from

814 complex environmental samples. *Elife* 6, 1–20. doi:10.7554/eLife.26580.

815 Zengler, K., and Zaramela, L. S. (2018). The social network of microorganisms - How

816 auxotrophies shape complex communities. *Nat. Rev. Microbiol.* 16, 383–390.

817 doi:10.1038/s41579-018-0004-5.

818

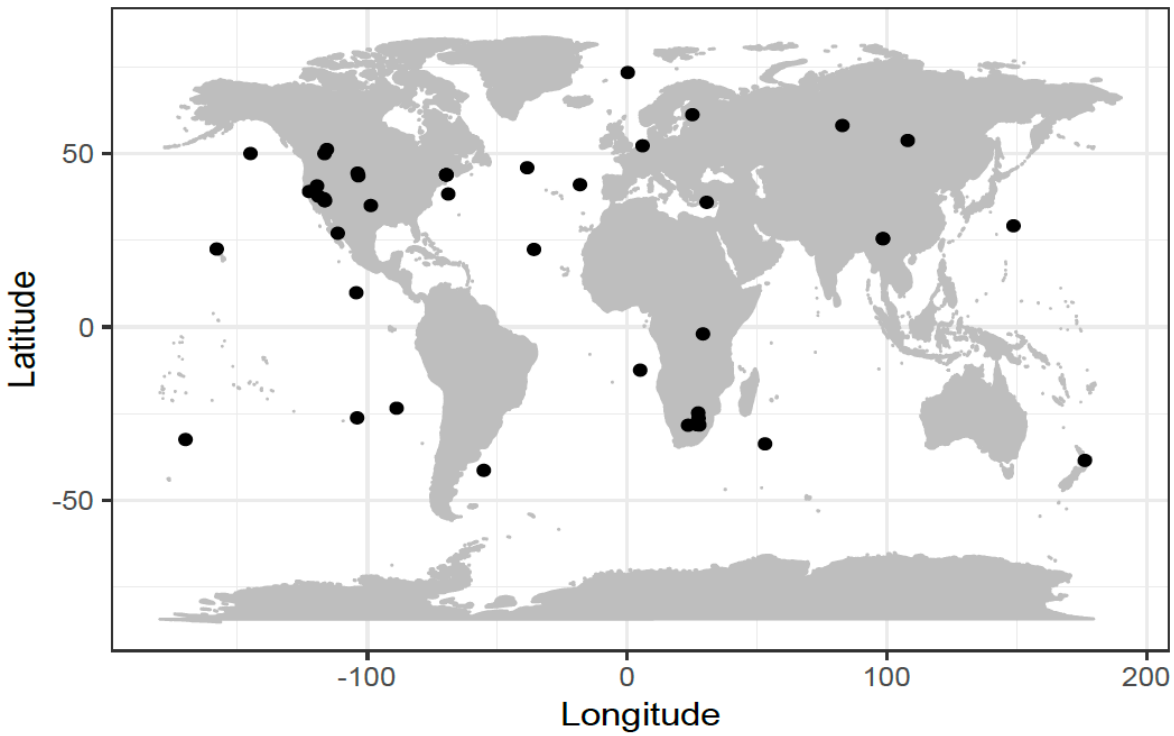

Figure 1. Geographic locations of sample collection sites.

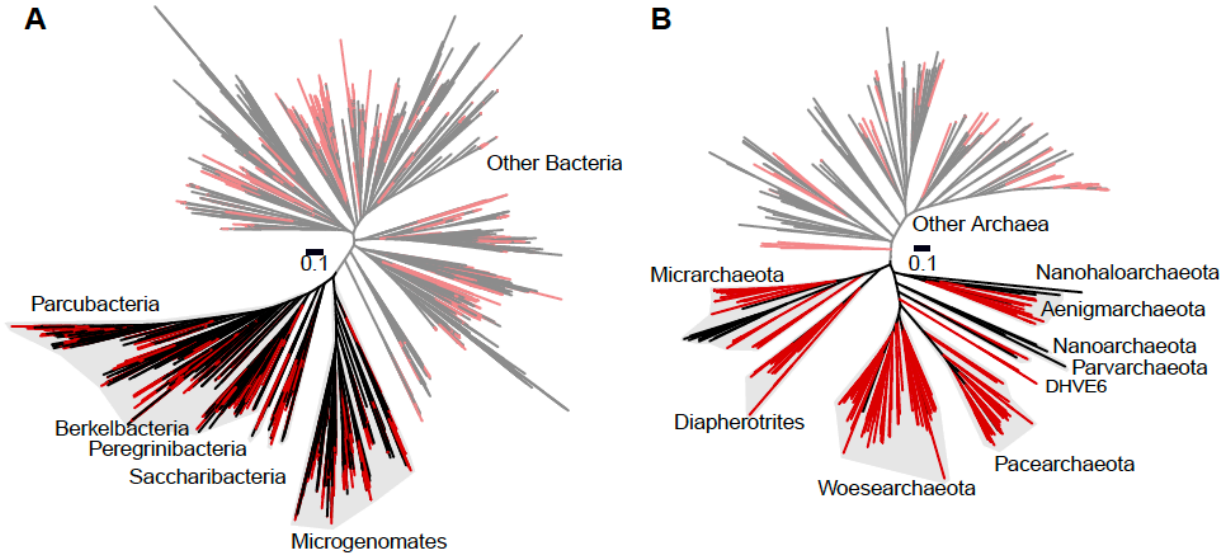

Figure 2. Maximum likelihood concatenated phylogenetic tree of single copy proteins (n=5) from Bacteria (a) and Archaea (b). All SAGs from this study are highlighted red. Patescibacteria and DPANN are highlighted with grey and labeled by individual proposed phyla within the superphylum (Rinke et al., 2013; Brown et al., 2015).

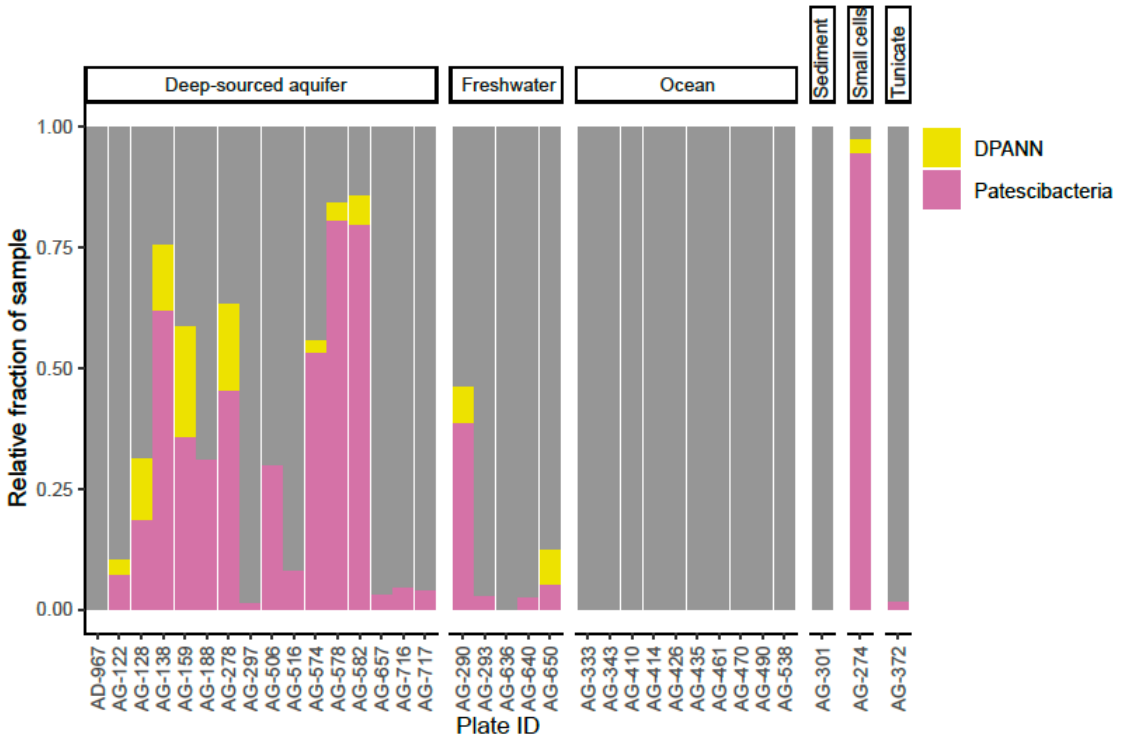

Figure 3. Relative abundance of Patescibacteria and DPANN from 34 geographically diverse samples determined from randomly sequenced LoCoS SAGs. The plate identifiers can be cross-referenced with specific SAGs and geographic sites in Table S1. The AG-274 sample contains small cells from a water-filled rock fracture at 1,340 m depth below surface in the Beatrix gold mine in South Africa.

855 **Figure 4.** Plot of the percent contribution of individual phyla to the Chi-square statistic from
856 checkM (**A**) and 16S rRNA gene (**B**) co-sorting analyses. Classification of phyla in (**A**) from
857 concatenated phylogenetic tree in Figure 2 (Table S1) and from 16S taxonomy in (**B**).

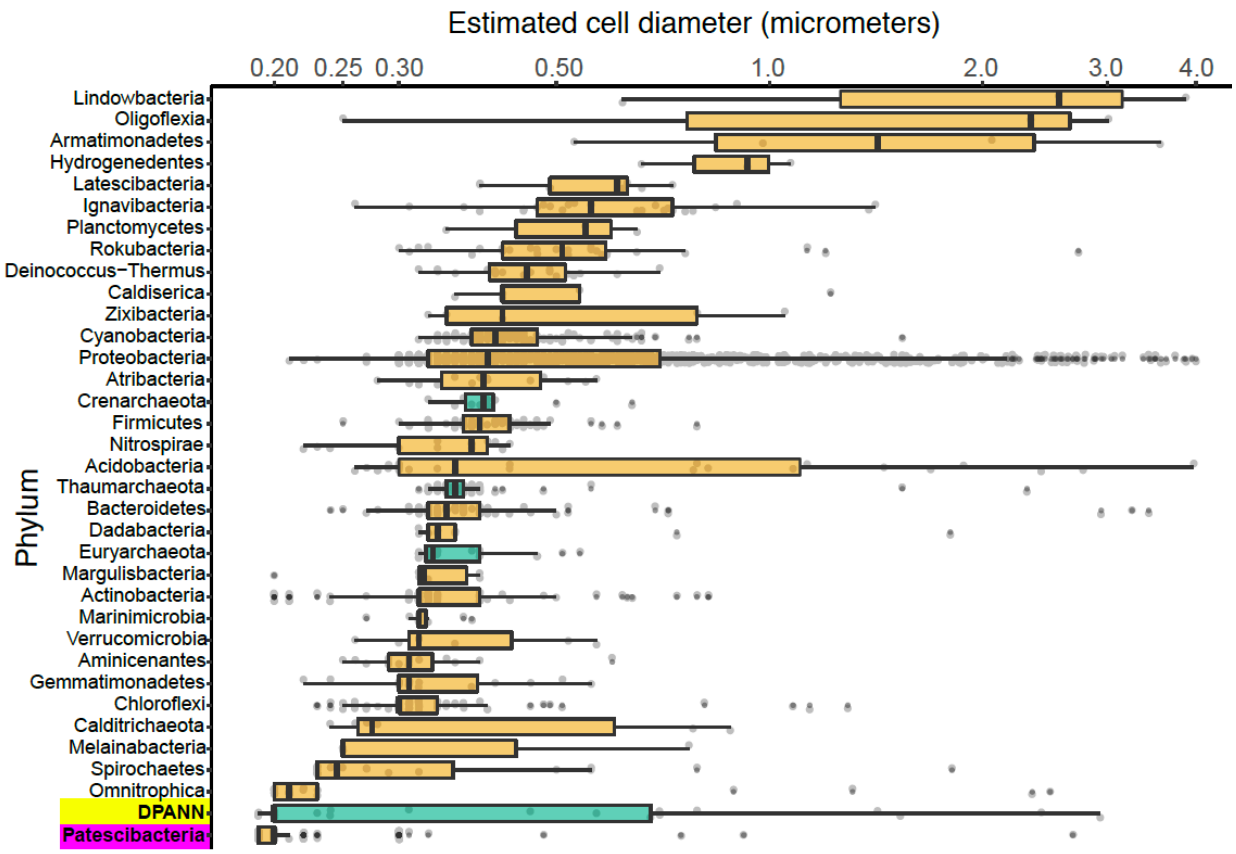

Figure 5. Phylum-resolved cell diameters. Solid black bars indicate medians; boxes represent the interquartile ranges (IQR) of the 1st (Q1) and 3rd (Q3) quartiles; whiskers denote the minimum (Q1 - 1.5*IQR) and maximum (Q3 + 1.5*IQR) values; outliers outside of the whiskers are marked by black dots. Orange indicates Bacteria and green indicates Archaea. A pairwise ranked-sum Wilcoxon test confirmed that the median diameter of Patescibacteria (highlighted in magenta) was smaller than most other phyla (27/36 phyla with p-values < 0.05; Table S5). The median diameter of DPANN (highlighted in yellow) was not significantly different from other archaea (1/36 phyla with p-values < 0.05; Table S5), likely due to the large variability in DPANN cell diameters. Individual cell diameters are available in Table S1 and pairwise p-values are located in Table S5.

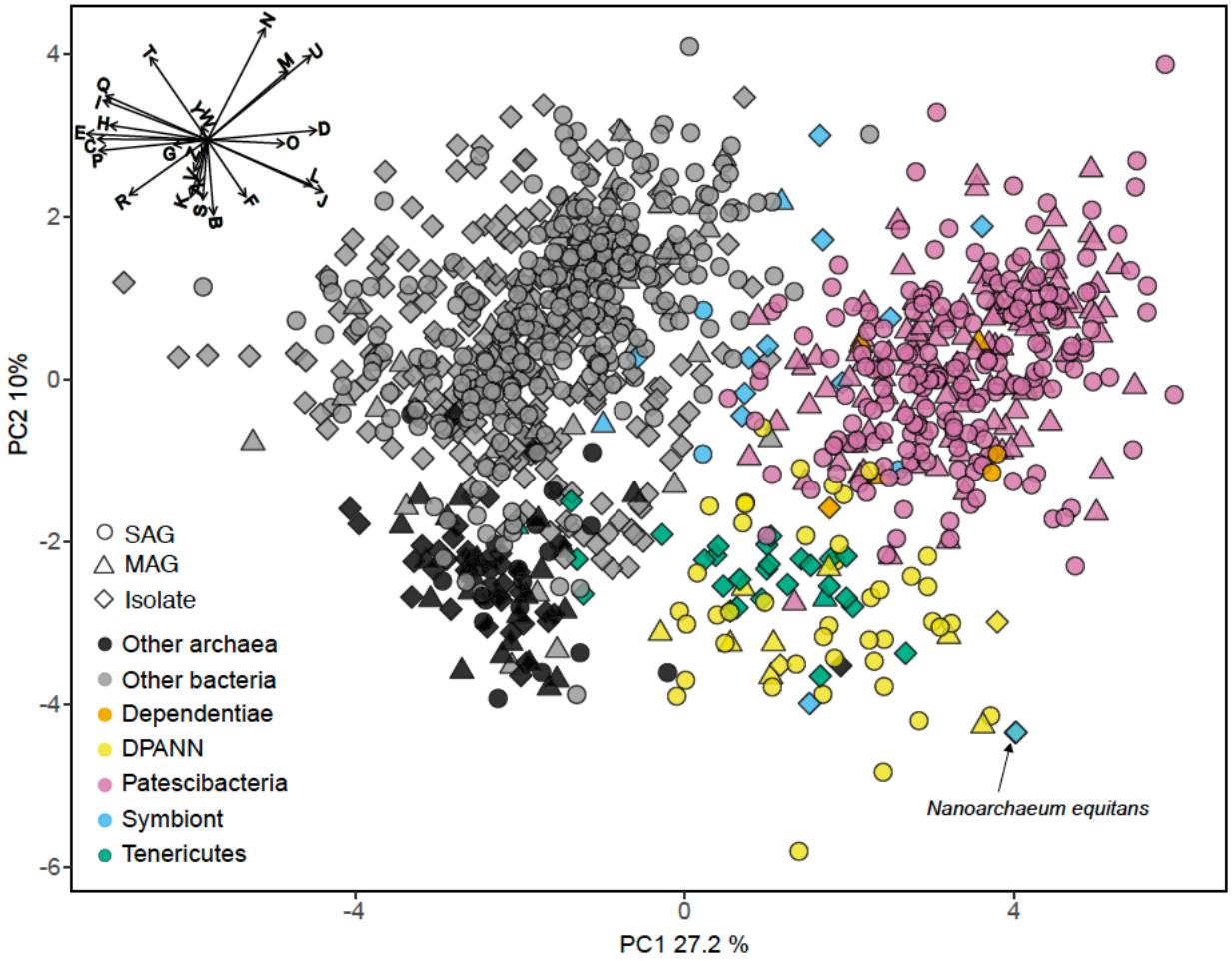

Figure 6. Principal components analysis (PCA) of the relative abundance of clusters of orthologous groups (COG) categories as the input variables. SAGs from this study (Table S1) and other studies (Table S2) with >30% completeness and had a near-full-length 16S rRNA gene and were included in the phylogenetic tree in Figure 8 (n=1,092). The vector plot in the upper left corner shows the COG categories that contributed to the most separation of the genomes: **Information Storage and Processing** Translation, ribosomal structure and biogenesis (J), RNA processing and modification (A), Transcription (K), Replication ,recombination and repair (L), Chromatin structure and dynamics (B); **Cellular Processes and Signaling** Cell cycle control, cell division, chromosome partitioning (D), Nuclear structure (Y), Defense mechanisms (V), Signal transduction mechanisms (T), Cell wall/membrane/envelope biogenesis (M), Cell motility (N), Cytoskeleton (Z), Extracellular structures (W), Intracellular trafficking, secretion, and vesicular transport (U), Posttranslational modification, protein turnover, chaperones (O); **Metabolism** Energy production and conversion (C), Carbohydrate transport and metabolism (G), Amino acid transport and metabolism (E), Nucleotide transport and metabolism (F), Coenzyme transport and metabolism (H), Lipid transport and metabolism (I), Inorganic ion transport and metabolism (P), Secondary metabolites biosynthesis, transport and catabolism (Q),; **Poorly Characterized** General function prediction only (R), Function unknown (S). SAG, single amplified genome; MAG, metagenome assembled genome. Symbiont genomes are listed in Table S4. Note position of *Nanoarchaeum equitans* with black arrow.

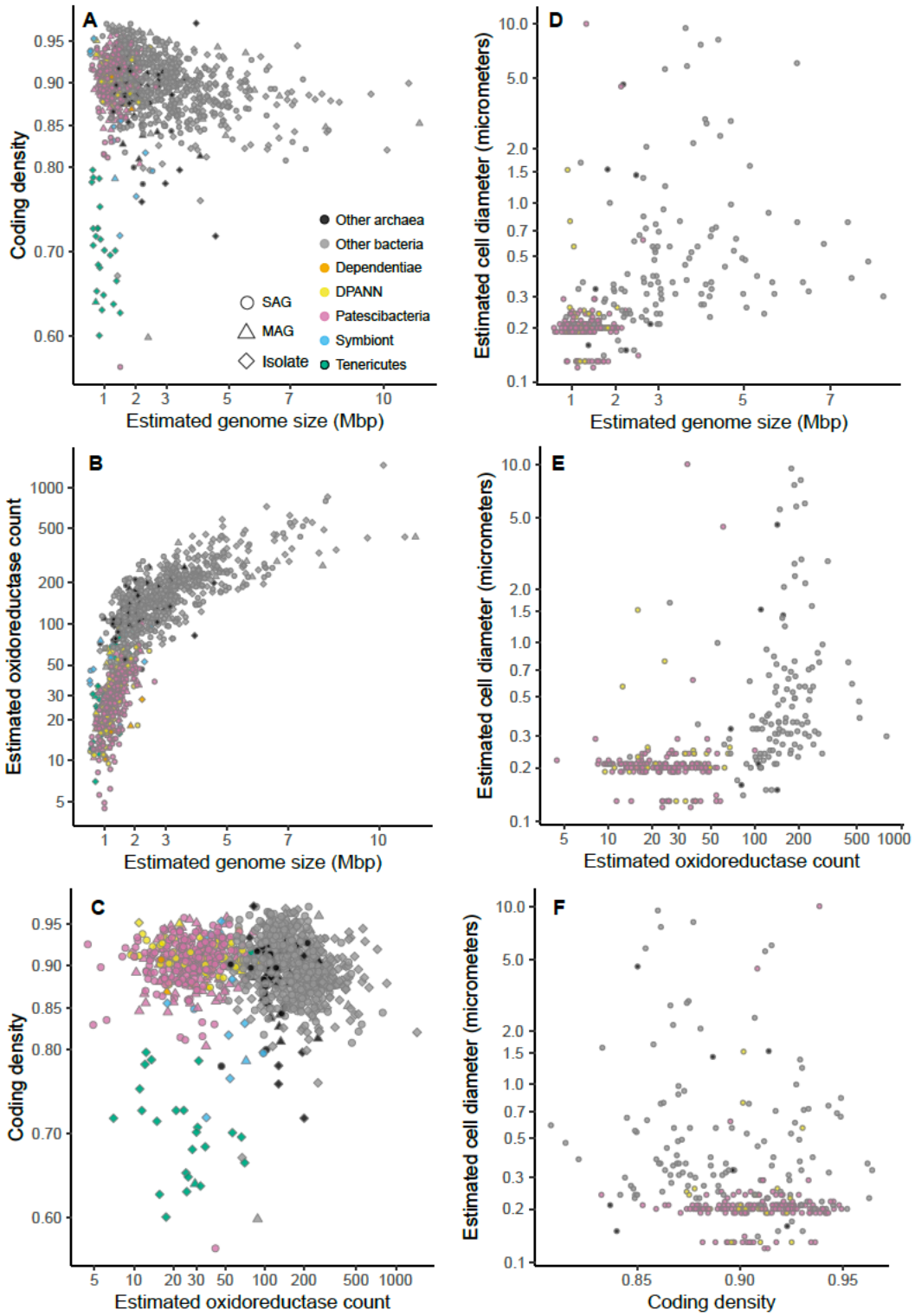

888 **Figure 7.** Relationship plots between estimated genome size, coding density, oxidoreductase
889 count, and cell diameter among SAGs (Table S1) and other genome sequences (Table S2) that
890 were greater than or equal to 30% complete, and were included in the 16S rRNA gene tree in
891 Figure 8. Symbiont genomes are listed in Table S4.

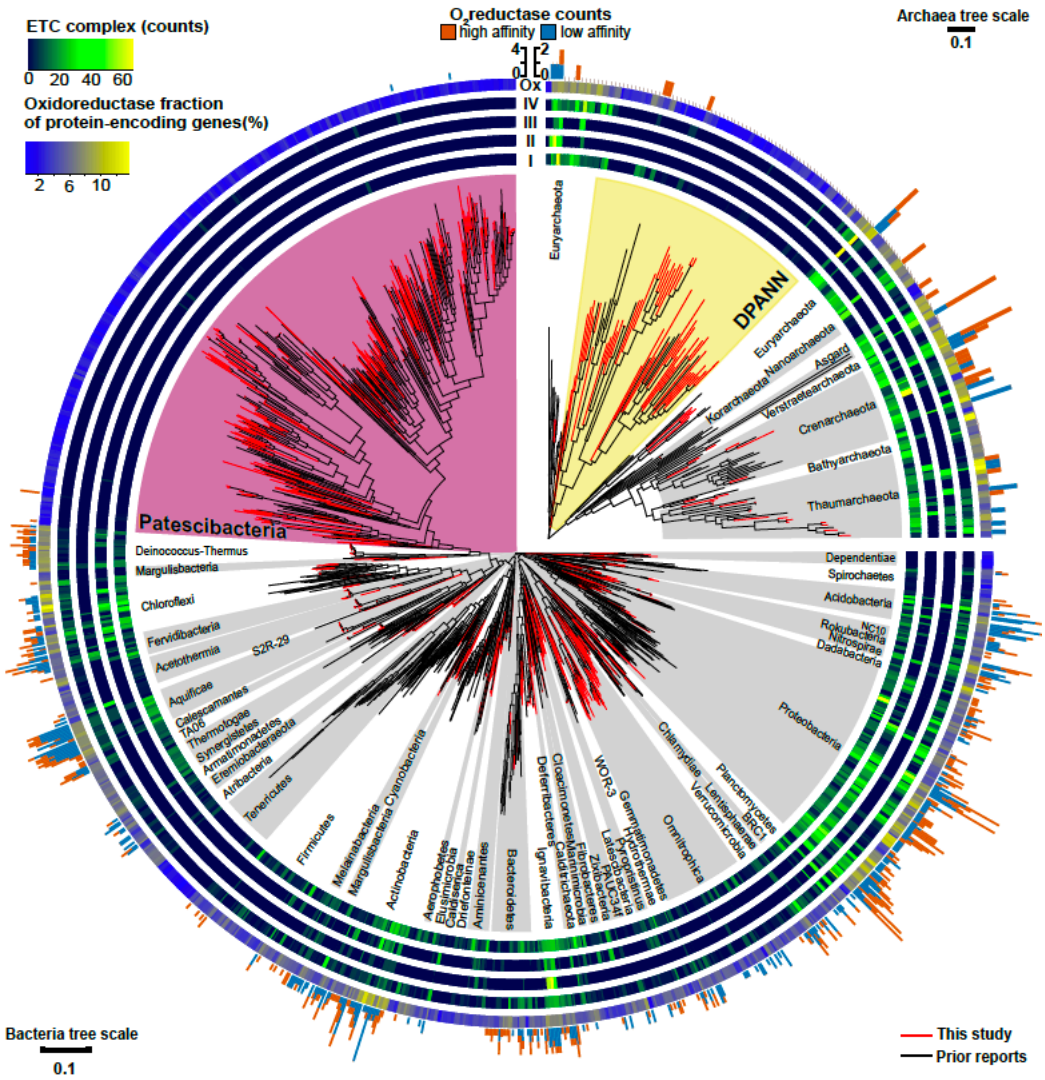

892 **Figure 8.** Maximum likelihood phylogeny of near full-length (>1,200 bp) 16S rRNA genes from
893 Bacteria and Archaea, annotated with the distribution of counts for electron transport chain
894 complexes, oxygen reductases, and oxidoreductase (Enzyme Commission 1; EC1) relative
895 abundances from SAGs in this study (Table S1) and previously reported genome sequences
896 (Table S2). The four innermost rings depict the counts of the electron transport chain complexes:
897 I (NADH dehydrogenase subunits), II (succinate dehydrogenase subunits), III (cytochrome c
898 reductase subunits), and IV (oxygen, nitrate, sulfate, iron, arsenate, and selenate reductase
899 subunits). The outermost ring shows the relative abundance of oxidoreductases (Ox) for each
900 genome assembly as a gradient from low (blue) to high (yellow). The peripheral stacked bar
901 charts show the counts of oxygen reductases from both the heme copper oxidase and bd-
902 ubiquinol oxidase oxygen reductase (O_2red) families grouped as high (orange) or low (sky blue)
903 affinity for oxygen (note scale bar differences between bacterial and archaeal trees).
904 Patescibacteria are highlighted in magenta and DPANN are highlighted in yellow. Other
905 bacterial and archaeal phyla are highlighted in alternating white and grey.

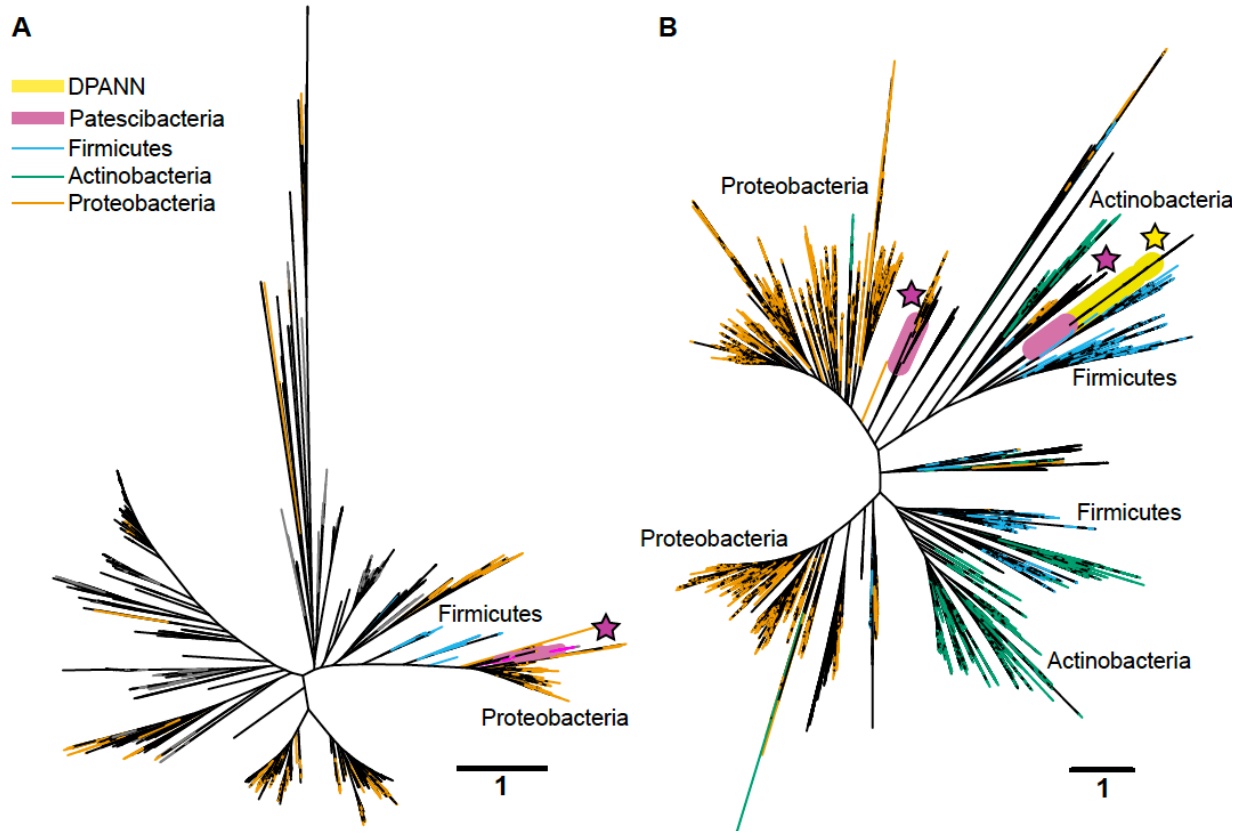

906 **Figure 9.** Maximum likelihood phylogenetic trees of the oxygen-binding subunit I from the
907 heme copper oxidase (HCO) type A (a) and the A subunit from the bd-ubiquinol (b) oxygen
908 reductase families. Patescibacteria and DPANN sequences are marked with magenta and yellow
909 stars, respectively. The Patescibacteria HCO type A sequences (a) are nested within a larger
910 clade containing mostly Proteobacteria (orange), and the Patescibacteria and DPANN bd-
911 ubiquinol sequences (b) are nested within Proteobacteria (orange) and Firmicutes (blue)
912 dominated clades. The scale bar represents the estimated number of substitutions per site

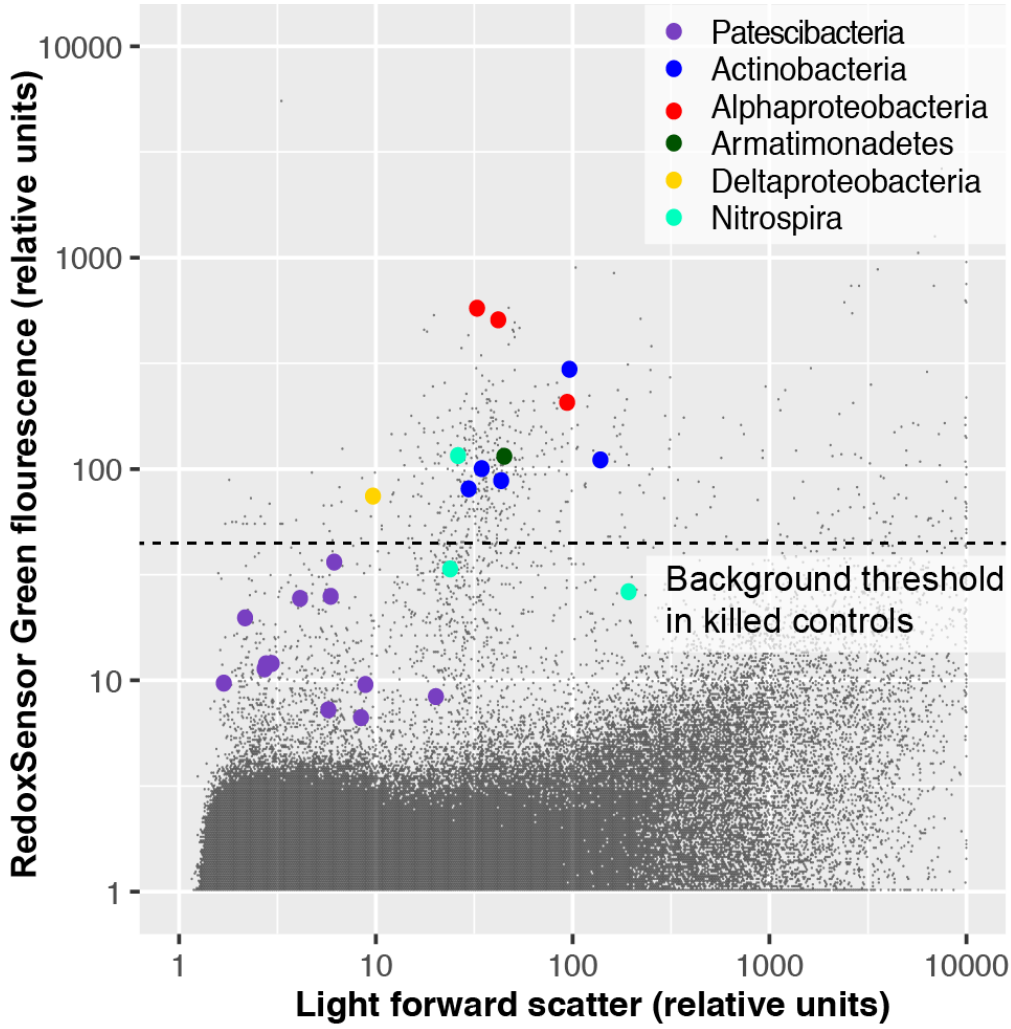

Figure 10. Oxidoreductase activity in subsurface (~300 m below surface) microbial cells from Homestake Mine (Lead, South Dakota, USA) measured by RedoxSensor Green (RSG; ThermoFisher).

Supplemental Table Captions

Table S1. Deep-sequenced and LoCoS SAGs from this study with genomic statistics and associated environmental metadata. Data are ordered with the following column headers:
1=genome; single amplified genome (SAG identifier)
2=gold.analysis.id; Gold analysis identifier (used to search genome in IMG/M)
3=phylum
4=assembly.completeness; checkM completeness estimates
5= contamination; checkM estimated genome contamination
6=assembly.size; SAG assembly size
7=est.genome.size; estimated genome size
8=coding.density
9=ec1.count; counts of oxidoreductases from SAG assembly
10=est.ec1.count; estimated counts of oxidoreductases from predicted genome size of n Mbp
11=16s.copy.number; number of predicted 16S rRNA genes
12=cell.diameter; estimated cell diameter
13=sequencing.center
14=sample.collection.site; name of site where samples were collected
15=sample.type
16=date.collected; sample collection date dd/mm/yy
17=latitude
18=longitude
19=depth
20=dissolved.oxygen (micromoles/L)
21=ph
22=salinity (practical salinity units, psu)
23=temperature (degrees Celsius
24=h2s; dissolved hydrogen sulfide (millimoles/L)
NA=not applicable

Table S2. Genomes from other studies with associated genomic statistical information (accessed from IMG/M on April 2018).

Table S3. Potential co-sorted SAGs from deep-sequenced and LoCoS datasets. SAGs can be cross-referenced for specific information with Table S1.

Table S4. Symbiont genome assemblies and taxonomic names used in Figures 6 and 7.

Table S5. Pairwise Wilcoxon's test p-values on all phyla versus phyla cell diameter estimations in Figure 5.